International Journal of Engineering Research and Development

DOI: 10.29137/ijerad.1974476
Volume:18 Issue:5 Pages:188-204 September/2026

Research Article

Online Geometric Quality Control of Precision Sequential Fiber Optic Wire Winding Using Multi-Angle Image Processing

Tolga Altın[*1,2], **Sadettin Orhan** [1], **Eren Ergül** [2]

[1]Department of Mechanical Engineering, Ankara Yıldırım Beyazıt University, 06010 Ankara, TÜRKİYE
[2]Ekinoks-AG Savunma Sanayi ve Tic. A.Ş., 06010 Ankara, TÜRKİYE

Received: 19/06/2026 **Revised**: 26/07/2026 **Accepted:** 30/07/2026

**** Corresponding Author:*** ***235103107@aybu.edu.tr***

Abstract

Precision sequential wire winding is widely employed in critical manufacturing applications, including fiber-optic and specialty cable production. Irregular winding structures may cause sudden interlayer tension increases during unwinding, leading to wire breakage and communication failure. In conventional processes, defects are identified only after operation completion, resulting in inevitable material and time losses. This study presents an image-processing-based online geometric quality control system for real-time winding monitoring. The coil is inspected from 12 viewing angles at 30° intervals; brightness profiles are extracted from multiple horizontal rows within a region of interest (ROI) and analyzed using adaptive moving-average thresholding. Sub-threshold regions are marked as potential defect zones, and classification is based on the maximum width (d) of consistently detected regions: Normal, Warning, or Fault. The method was validated on a 2 mm diameter fiber-optic wire with 93 rows per layer. Defects with $d < 6$ pixels (≈0.40 mm) were classified as Normal, $6 \leq d \leq 13$ pixels (≈0.40–0.80 mm) as Warning, and $d > 13$ pixels (≈0.80 mm) as Fault. The results obtained from 20 winding layers demonstrated that the proposed method can reliably detect winding defects, achieving an 85% agreement with operator assessments. Furthermore, under a conservative worst-case binary evaluation, the method attained an accuracy of 90.0% and a recall of 100.0%, highlighting its robustness in identifying defective winding conditions.

Keywords

Precision sequential fiber optic wire winding, image processing, anomaly detection, brightness profile analysis, online quality control, multi-angle image acquisition.

How to cite this article:

Altın, T., Orhan, S., & Ergül, E. (2026). Online geometric quality control of precision sequential fiber optic wire winding using multi-angle image processing. International Journal of Engineering Research and Development, 18(5), 188–204. https://doi.org/10.29137/ijerad.1974476

This is an open access article under Creative Commons Attribution-NonCommercial-NoDerivatives 4.0 (CC BY-NC-ND 4.0) International License.

1. Introduction

Precision wire winding is a critical manufacturing process employed in high-reliability applications such as fiber optic sensors, specialized communication cables, and defense systems. The fiber optic wires considered in this study are utilized for communication purposes in systems where the wire is unwound from a coil at high speeds in accordance with the motion of the platform. In such applications, geometric irregularities arising during the winding process—including pitch deviations, wire overlaps, and gap shifts—can lead to sudden increases in tension in wire layers during unwinding. These tension fluctuations may cause wire breakage, resulting in communication failure. Since communication loss in these systems often implies a complete loss of operational control without the possibility of external intervention, ensuring high winding quality is critical for system reliability and mission success.

Conventional quality control methods for coil winding predominantly rely on post-process mechanical testing. These methods typically require the wound coil to be opened and inspected, rendering the tested wire permanently unusable. Consequently, such approaches not only lead to significant material and time losses but also necessitate scrapping the inspected coil. Moreover, they provide limited diagnostic information regarding the exact location, layer, or winding angle at which a defect has occurred.

In recent years, image processing and machine vision technologies have become widely adopted in manufacturing quality control applications. Tang et al. (2023) presented a comprehensive review of machine-vision-based surface defect detection methods, covering image preprocessing, region-of-interest (ROI) detection, segmentation, feature extraction, and defect classification techniques. Zhang et al. (2021) proposed a grayscale image analysis and template-matching approach for detecting surface defects in steel wire ropes, demonstrating robustness against noise and illumination variations. Moru and Borro (2020) developed a machine-vision-based inspection system for the dimensional and geometric quality control of gears. Xu et al. (2023) introduced a non-contact machine-vision method for measuring transformer winding tilt angles and achieved high measurement accuracy through image-processing techniques. Similarly, Guo and Yang (2014) proposed an image-processing-based defect detection approach for fiber optic gyroscope coil winding, successfully identifying stacking, cut, and uneven winding defects using mathematical morphology and moving-target detection algorithms.

Beyond fiber optic winding, machine vision-based defect detection has been widely investigated across various manufacturing applications. For example, Zhou et al. (2023) reviewed machine vision-based inspection techniques for printed circuit boards, while Rasheed et al. (2020) presented a comprehensive survey of computer vision approaches for fabric defect detection in the textile industry. These studies further demonstrate the broad applicability of image processing-based quality inspection techniques across diverse industrial sectors.

The specific challenges associated with precision fiber optic winding and its automation requirements have also been addressed in earlier studies (Hung and White, 1992a; 1992b). Layer slippage and winding density instability have been identified as major quality issues in fuzzy logic-based precision winding systems (Siddiqui et al., 2020). Although stress-based approaches have been proposed for detecting collapse defects in winding structures, these methods operate independently of image-processing techniques (Zhang et al., 2024). Despite the growing interest in machine vision applications, studies focusing on image-processing-based quality control of sequential fiber optic wire winding remain limited.

More recently, image-based and deep learning-based techniques have been increasingly applied to winding and cable manufacturing processes. Zhao et al. (2024) proposed an improved MobileNetV1-based classifier for identifying gap and stack defects during fiber optic coil winding, while Zhuo et al. (2024) developed a real-time machine vision system for the simultaneous surface defect inspection and geometric measurement of spiral cylindrical coils. In optical cable manufacturing, Gou et al. (2024) introduced an online machine vision method for detecting pitch defects, whereas Chen et al. (2016) presented an infrared illumination-based inspection approach that exploits grayscale intensity variations to identify surface defects in optical cables. Similarly, Grün et al. (2025) reported an inline monitoring system for filament-wound composite pressure vessels by integrating line-scan imaging with geometric deviation analysis.

In contrast to these approaches, which either rely on deep learning models requiring large amounts of labeled training data or employ specialized imaging hardware such as line-scan or infrared systems, the proposed method is based on a training-free, physically interpretable adaptive thresholding algorithm implemented using a conventional USB camera. This design enables straightforward deployment with minimal calibration requirements while maintaining an effective capability for detecting winding irregularities.

A review of the existing literature reveals that most image-based inspection systems either rely on images acquired from a single viewing angle or focus exclusively on surface-level defects. Furthermore, quality assessment of fiber optic winding structures is generally based on strain measurements or destructive mechanical inspection methods, while image-processing approaches have primarily been applied to other industrial components. To the best of the authors' knowledge, an online quality control methodology employing multi-angle image analysis for sequential fiber optic wire winding structures has not been comprehensively investigated.

Therefore, the primary contribution of this study is the online detection of localized winding irregularities through multi-angle brightness profile analysis combined with adaptive thresholding techniques.

To address this gap, this study proposes a nondestructive, image-processing-based online geometric quality control system capable of identifying irreversible winding faults during production, issuing real-time warnings to the operator, and evaluating each winding layer independently before progression to subsequent layers. The proposed system requires only minimal calibration data and does not depend on large training datasets. Images are acquired from twelve different viewing angles at 30° intervals, providing complete coverage of the winding surface. Quality assessment is performed by analyzing the average brightness profiles obtained from multiple horizontal rows within a user-defined ROI encompassing the winding region. Regions exhibiting brightness values below an adaptive threshold are identified, and the widths of these low-brightness regions are used to classify the winding condition as Normal, Warning, or Fault. Threshold values are determined through physical calibration measurements and are defined as 0.40 mm and 0.80 mm for Warning and Fault conditions, respectively.

The remainder of this paper is organized as follows. Section 2 describes the overall system architecture and hardware infrastructure. Section 3 presents the proposed image processing methodology in detail. Section 4 discusses experimental results and performance evaluation. Finally, Section 5 summarizes the main findings and outlines potential directions for future research.

Symbols and Abbreviations

µm	Micrometer
mm	Millimeter
px	Pixel
P	Pitch (Center to Center Distance)
p	Pixel density (px/mm)
FOV	Field of View
ROI	Region of Interest
RGB	Red, Green, Blue
R_W	Number of horizontal pixels in the image (px)
W_{FOV}	Experimentally measured horizontal field-of-view width (mm)
d	Maximum width of the low-brightness region (px)
d_{px}	Pixel width of the wire in the image (px)
d_{wire}	Physical diameter of the wire (mm)
N	Number of horizontal analysis rows
B(x)	Average brightness profile along the x-axis (grayscale levels)
MA(x)	Moving-average brightness profile (grayscale levels)
W	Moving-average window size (px)
T(x)	Adaptive threshold value (grayscale levels)
Δ	Adaptive threshold offset (grayscale levels)

2. System Description

The quality control system proposed in this study has three main components: an image acquisition unit, lighting infrastructure, and image processing software. The system is based on the principle of rotating the coil at 30° intervals along the radial axis after each winding stage is completed, photographing it from 12 different angles, and analyzing the obtained images online. The image processing software processes the raw images received from the camera via USB connection, generating a Normal, Warning, or Fault decision at the end of each stage and informing the operator. The general structure of the system architecture is presented in Figure 1, and the hardware and physical parameters used are presented in Table 1.

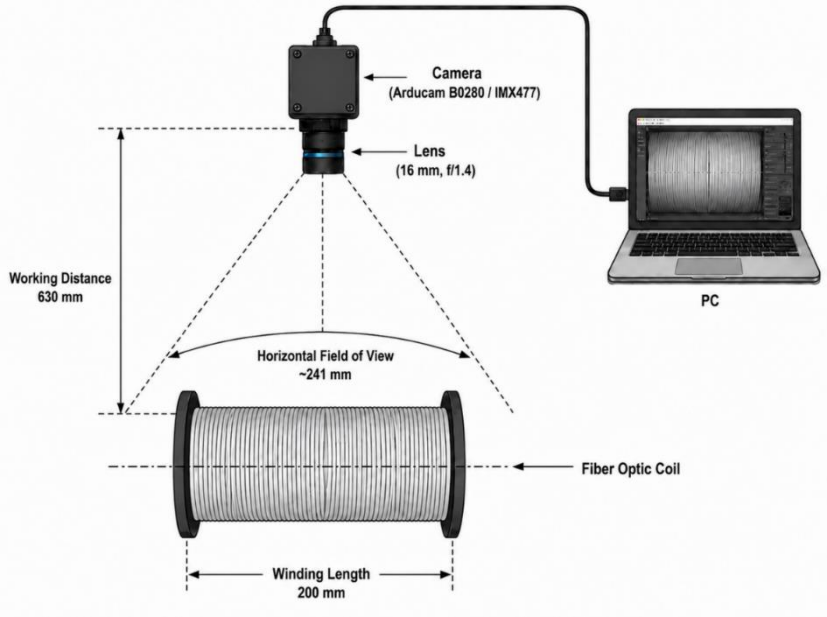

Figure 1. System Hardware Architecture

Table 1. System Parameters

Parameter	Value
Sensor Resolution	3840 x 2160 px
Pixel Size	1.55 µm
Focal Length	16 mm
Working distance	630 mm
Horizontal FOV	241 mm
Pixel Density	15.93 px/mm
Angular interval	30°
Number of Angles per Layer	12
Total Processed Images	240
Number of Layers	20
Total Wire Length	820 m
Wire diameter	2 mm
Pitch	2.151 mm
Free Gap	151 µm
Winding Length	200 mm
Number of Rows	93
Warning Tolerance	0.40 mm
Fault Tolerance	0.80 mm

2.1. Camera and lens system

In this study, a high-resolution imaging system was used to analyze the coil geometry. The imaging infrastructure was created using an Arducam 12MP USB Camera (B0280, with IMX477 sensor) and a Raspberry Pi 16mm Telephoto Lens (SC0123). A 16mm telephoto lens was preferred over the camera's standard 6mm lens; thus, sufficient pixel density and depth of field were achieved at a working distance of 630 mm (Table 1).

The camera was positioned perpendicular to the coil axis, and the working distance was determined to be approximately 630 mm. This distance was experimentally optimized to both image the entire winding surface and maintain sufficient pixel density. The optical system used provides a horizontal field of view of approximately 241 mm; thus, the entire coil region with a length of 200 mm can be imaged in a single image.

To make the wire geometry on the winding surface more prominent, the lighting system was created using a linear light source placed in an appropriate location. Thanks to this approach, shadowing effects on the wire surface were reduced, and the brightness profile analysis was performed more stably.

2.2. Optical calibration

Pixel-distance calibration was performed to relate image processing results to physical tolerances. During the calibration process, the experimentally measured horizontal field of view was used as a physical reference. Pixel density was calculated as the ratio of the number of horizontal pixels in the image to the width of the physical field of view using the equation 1.

$$p = \frac{R_W}{W_{FOV}} \tag{1}$$

Where: p, Pixel density (px/mm), R_W, Number of horizontal pixels, W_{FOV}, experimentally measured horizontal field of view width. p is calculated as 15.93 px/mm.

This conversion factor also reveals the geometric resolution of the system. Accordingly, a physical length of 1 mm is represented as 15.93 pixels in the image. The pixel width of a 2 mm diameter wire in the image has been calculated with equation 2.

$$d_{px} = d_{wire} \times p \tag{2}$$

Where: d_{px}, pixel width of the wire in the image, d_{wire}, physical diameter of the wire. Thus, brightness deviations measured on the image can be correlated with physical tolerance values, and pixel-based anomaly detection obtained from the algorithm gains physical meaning.

2.3. Physical parameters

The coil examined in this study consists of 2 mm diameter coated fiber optic wire with a theoretical pitch of 2.151 mm. This value is obtained by placing 93 rows of wire in a winding length of 200 mm. The free space between adjacent wires is approximately 151 μm, and this value constitutes the basic reference point in determining the sensitivity limit of the system. The coil consists of a total of 20 winding layers. All physical parameters are presented together in Table 1.

A sample winding image of the coil under investigation is given in Figure 2. The image shows the regular arrangement of the wire rows and the general characteristics of the winding structure.

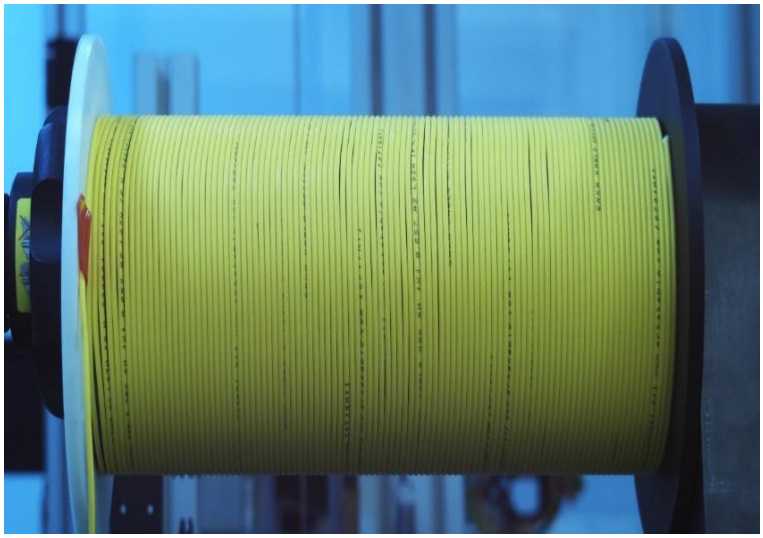

Figure 2. Sample Image of the Fiber Optic Coil Winding Structure

2.4. Image acquisition strategy

The proposed system utilizes a multi-angle imaging approach to physically visualize the entire winding surface. When each winding layer is completed, the coil circumference is imaged from a total of 12 different angles, ranging from 0° to 330°, at 30° angular intervals. This allows for the complete scanning of the coil circumference and reduces blind spots that may occur during single-angle imaging.

All images are obtained under the same camera configuration, lens parameters, working distance, and lighting conditions. This ensures that the physical imaging conditions remain constant between images taken from different angles. Each image corresponds to a different

radial region of the winding surface. In the obtained images, wire surfaces generally appear brighter, while gaps, local increases in wire spacing, and winding irregularities are observed as darker regions due to changes in light reflection distribution. Images taken from 12 different angles for a single winding layer are shown in Figure 3.

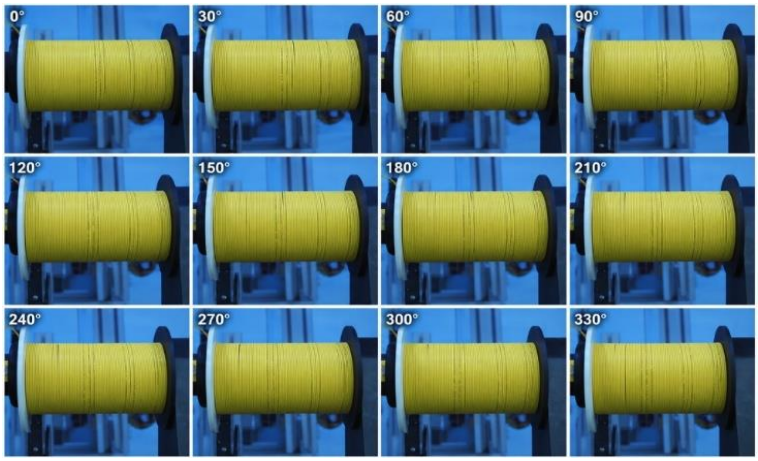

Figure 3. Images Acquired from 12 Different Angular Positions at 30° Intervals for a Single Winding Layer

3. Proposed Method

This study proposes an image processing-based quality control method developed for the online detection of geometric irregularities on the surface of sequentially wound fiber optic wires. The proposed algorithm consists of multi-angle image acquisition, ROI-based multi-row brightness profiling and consistency analysis, adaptive thresholding, and a decision mechanism. The system performs automatic classification such as Normal, Warning, or Fault by analyzing the winding surface after each winding layer is completed.

In the proposed method, the winding surface is imaged from a total of 12 different angles in 30° angular steps within the 0°–330° range at the end of each winding layer. Each acquired image is analyzed independently, and a quality decision is made for the relevant angle. Then, all angular images are evaluated together to determine the final quality status on a layer basis. Thus, the aim is to detect localized winding irregularities that are only visible from specific angles.

The algorithm first converts the RGB image to grayscale, then creates a ROI region using user-defined winding boundaries. Column-based average brightness profiles are extracted from the selected horizontal analysis rows within the ROI. Next, an adaptive thresholding method based on moving averages is applied, and regions below the threshold are marked as potential defect regions. Quality decisions are generated for each image using the maximum width of the low-brightness regions detected below the adaptive threshold. The overall quality decision is made by considering the worst-case scenario among all angular images, following the priority rule of Fault > Warning > Normal. The general flow of the proposed algorithm is given in Figure 4.

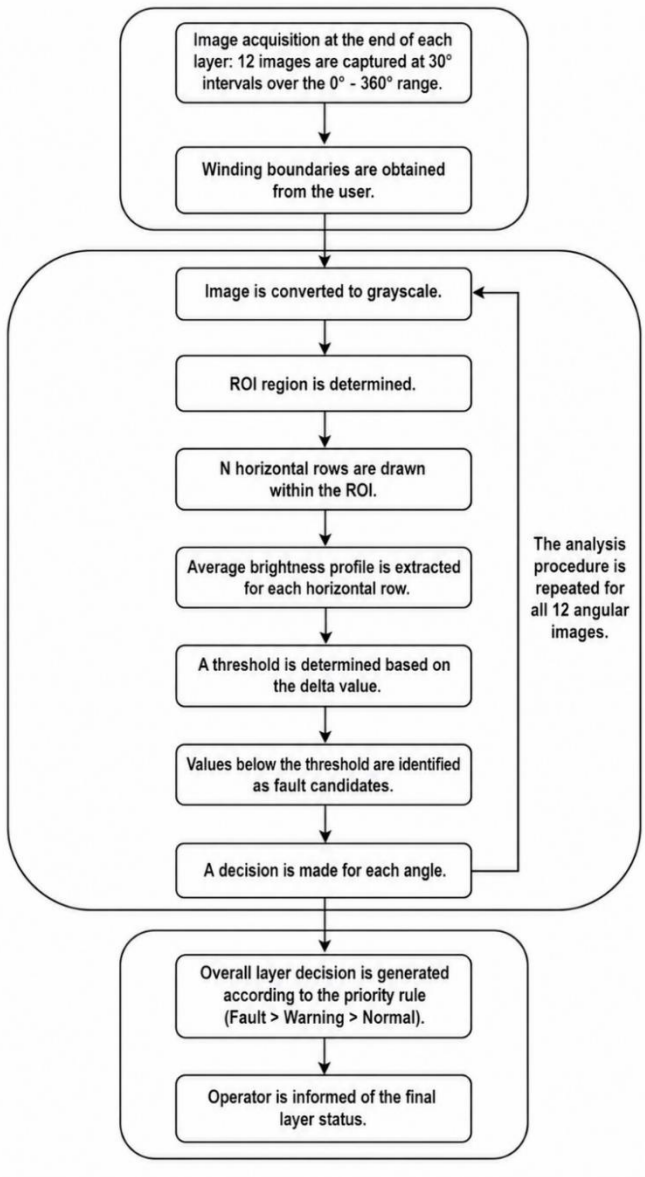

Figure 4. General Flow of the Proposed Algorithm

3.1. Multi-angle image evaluation approach

In the proposed method, each angular image obtained from the winding surface is analyzed independently. Since local geometric distortions occurring during the winding process only become visible at specific viewing angles, evaluating all angular images separately increases system reliability.

The 12 angular images obtained after each winding layer is completed are processed sequentially by the proposed algorithm. ROI determination, brightness profiling, adaptive thresholding, and anomaly detection are applied independently for each image. Thus, local winding irregularities that are not apparent at one angle can be detected from different angular images. After evaluating all angular images individually, the resulting decisions are combined to create a general layer status. In this way, the proposed method can perform both local analysis at the angular level and general quality assessment at the layer level.

3.2. ROI selection and brightness profiling

After the image acquisition process, each RGB image is converted to grayscale using the cvtColor function of the OpenCV library. Since the proposed method relies solely on brightness profile analysis, color information is unnecessary; grayscale conversion reduces computational load while preserving all the necessary intensity information for the analysis. This conversion applies the standard weighted brightness formula $Y = 0.299R + 0.587G + 0.114B$, which more accurately preserves perceived brightness differences compared to a simple channel average. The normal winding image and its grayscale conversion are presented in Figure 5.

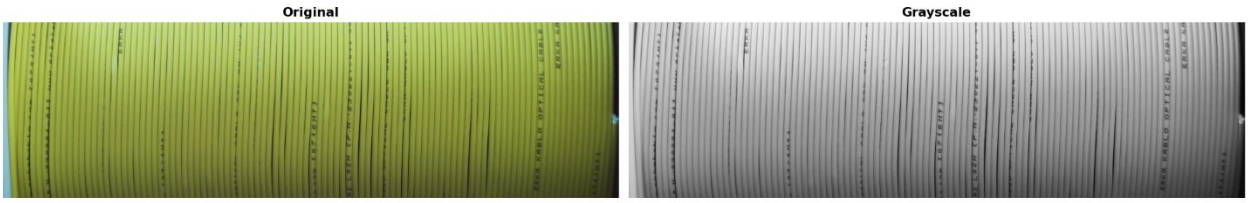

Figure 5. Original and Grayscale Images of the Winding Surface

Following grayscale conversion, the winding region is defined using a region of interest (ROI) whose coordinates are specified by the operator during the initial setup. These coordinates remain fixed throughout each measurement stage. However, as the winding process progresses, the accumulation of successive wire layers increases the coil diameter, resulting in gradual changes in the apparent size and position of the winding region within the captured images. Consequently, the ROI coordinates are periodically updated by the operator to ensure that the entire winding region remains within the analysis area. The location of the ROI in the captured image is illustrated in Figure 6.



Figure 6. ROI Region

Multiple horizontal analysis rows are selected within the defined ROI. Using multiple horizontal rows instead of a single horizontal row reduces the effect of local noise and small lighting variations, thus increasing system stability. For each horizontal row, the column-based average brightness profile along the x-axis is calculated with equation 3.

$$B(x) = \frac{1}{N}\sum_{i=1}^{N} I(y_i, x) \tag{3}$$

Where $I(y_i,x)$ represents grayscale intensity at coordinate (x,y_i), N is the number of analysis rows and B(x) is the average brightness profile.

In this study, N = 20 horizontal analysis rows were used. To determine the appropriate number of analysis rows, preliminary experiments were conducted using different values of N. When a small number of rows (e.g., N = 5) was used, the extracted brightness profiles became more sensitive to random noise and produced unstable results. Conversely, using many rows (e.g., N = 50) significantly increased the processing time without providing a noticeable improvement in detection performance. Based on these preliminary experiments, N = 20 was selected as an appropriate compromise between analysis stability and computational efficiency. The multiple horizontal analysis row approach is shown in Figure 7.

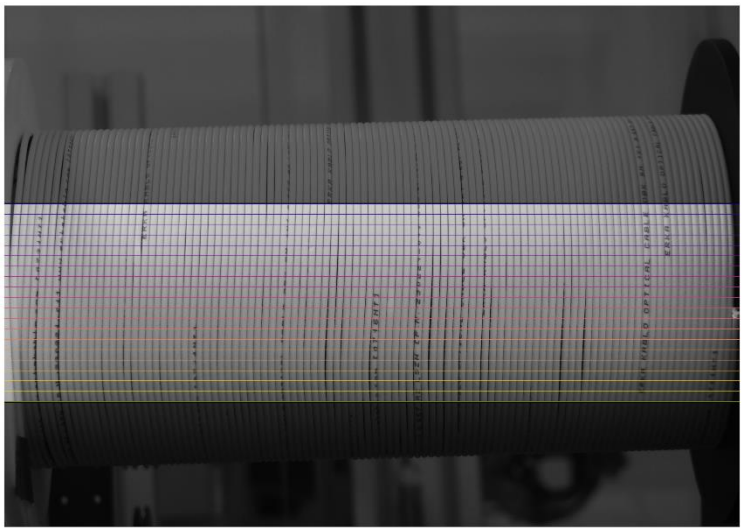

Figure 7. Multiple Horizontal Analysis Rows used for Brightness Profile Extraction within the ROI

3.3. Adaptive thresholding and decision mechanism

An adaptive thresholding method is applied to identify geometric irregularities on the winding surface using average brightness profiles obtained from the ROI region.

Due to light distribution, surface reflections, and wire geometry in the winding images, brightness values do not remain constant throughout the image. Therefore, instead of using a fixed threshold value, a moving average-based adaptive thresholding approach is preferred.

First, a moving average is calculated for each brightness profile at the determined window size. The moving average profile is expressed in equation 4.

$$MA(x) = \frac{1}{W}\sum_{x-W/2}^{x+W/2} B(k) \tag{4}$$

Where MA(x) represents the moving average profile, B(k) represents the brightness value in the relevant column, and W represents the moving average window size. An adaptive threshold profile is then created by extracting a specific Δ value from the moving average profile. It is given by equation 5.

$$T(x) = MA(x) - \Delta \tag{5}$$

Where T(x) represents the adaptive threshold value, and Δ represents the experimentally determined tolerance value. In this study,Δ = 10 was used, and the moving average window size was set to W = 1000 pixels.

The moving average window size (W) was determined through preliminary experiments using different window lengths. Small window sizes caused printed markings on the cable surface and local brightness fluctuations to affect the moving average profile, resulting in false candidate defect regions. In contrast, a window size of W = 1000 pixels effectively captured the overall illumination trend while suppressing the influence of cable markings, thereby preventing them from being falsely identified as defects. Accordingly, W = 1000 was adopted for all subsequent experiments.

The adaptive threshold offset (Δ) controls the sensitivity of the defect detection algorithm. During parameter optimization, the threshold profile was designed to remain slightly below the local minima of the moving average profile under normal winding conditions, thereby enabling the detection of brightness reductions associated with winding defects while minimizing false detections. Smaller values of Δ increased the sensitivity of the algorithm to noise and illumination variations, whereas larger values reduced its ability to detect subtle geometric irregularities. Based on the preliminary experiments, Δ = 10 provided the best trade-off between detection sensitivity and robustness and was therefore employed throughout the study. When the brightness profile falls below the threshold value, the corresponding region is identified as a potential defect area (B(x)<T(x)). Regions below the threshold generally correspond to geometric distortions such as wire spacing, local wire displacement, overlap, or winding irregularities.

In the proposed method, a single pixel falling below the threshold is not directly considered a defect. Instead, continuous regions below the threshold are detected, and only regions that consistently appear in multiple analysis rows at the same x-position are marked as defect candidates. This consistency analysis eliminates single-row drops caused by random noise, while true geometric distortions are revealed by repetition in the same x-position across multiple rows. The decision is made based on the maximum width (d) of these consistent regions. A candidate region is confirmed only when it is consistently observed at the same x-position in at least 5 of the N analysis rows. This criterion was introduced to reduce false detections arising from random noise and local illumination variations affecting individual analysis rows. Such artifacts typically appear sporadically and are confined to a limited number of rows, whereas genuine geometric irregularities are expected to produce consistent responses at similar horizontal locations across multiple neighboring analysis rows. Preliminary experiments indicated that requiring a candidate defect to be detected in at least five analysis rows effectively suppressed isolated false detections while preserving true geometrically significant irregularities. Accordingly, the minimum inter-row consistency criterion was set to five rows for all experiments. To suppress false positives due to coil flange boundaries, the leftmost ~40 pixels and rightmost ~50 pixels of the image are excluded from the analysis. Classification thresholds are defined in Table 2.

In this study, decision thresholds were determined by considering physical pitch deviations. Considering the resolution of the imaging system used, physical deviations of 0.40 mm and 0.80 mm correspond to approximately 6 pixels (6.37 px) and 13 pixels (12.74 px), respectively. Accordingly, the decision mechanism was created based on the threshold values given in Table 2.

Table 2. Decision Thresholds

Range	Decision
$d < 6$ px	Normal
$6 \text{ px} \leq d \leq 13$ px	Warning
$d > 13$ px	Fault

Where d represents the maximum width of the low-brightness regions below the adaptive threshold. This approach aims to differentiate between small brightness fluctuations and true geometric winding distortions.

3.4. General layer evaluation

After independently analyzing all 12 angular images, the final quality decision at the layer level is made. In the proposed method, the overall layer condition is determined by considering the worst-case scenario among all angular images. This approach prevents local winding irregularities, visible only from specific angles, from being overlooked during the final quality assessment. The decision priority used in this study is defined as Fault > Warning > Normal.

Accordingly, if any of the angular images are classified as "Fault," the relevant winding layer is directly classified as Fault. If no Fault condition is found but at least one image is in the "Warning" class, the overall layer is classified as Warning. If all angular images are evaluated as Normal, the relevant layer is considered Normal.

This approach increases the reliability of the quality control system by preventing the overlooking of local geometric irregularities. Finally, the generated layer decision is communicated to the operator for online monitoring of the winding process.

4. Experimental Results and Discussion

Experimental validation was conducted using a single fiber optic coil comprising 20 winding layers, corresponding to an approximate wound wire length of 820 m. Upon completion of each winding layer, images were acquired from 12 uniformly distributed angular positions, yielding a total of 240 images for analysis. Although the proposed algorithm processes each image independently, the final quality assessment for a winding layer is obtained by integrating the results from all 12 angular views. Consequently, the performance evaluation was performed at the layer level, resulting in 20 independent evaluation samples rather than 240 image-level samples.

The reference assessment was established by two experienced operators with 7 and 3 years of expertise in precision winding processes, respectively. To ensure an unbiased evaluation, the operators performed the inspection without access to the outputs of the proposed method. Each winding layer was jointly examined, and a consensus decision was reached by classifying the layer as either Normal or Fault. The inspection procedure consisted of an initial visual examination followed by dimensional verification of suspicious regions using calipers and precision gauges. The resulting consensus classifications were adopted as the ground-truth labels for evaluating the performance of the proposed method.

4.1. Normal winding analysis

The proposed image processing-based quality control method was first tested on Fault-free winding images. The aim at this stage was to examine whether the brightness profile extraction and adaptive thresholding method operates stably under normal winding

conditions. Since the geometric distribution of the wires remains similar across the surface in a regular winding structure, the brightness profiles obtained from the ROI region generally show a stable structure.

Figure 8 shows an example of a normal winding image and its corresponding brightness profiles. It was observed that the profiles obtained from multiple horizontal analysis rows were quite close to each other, and no large abrupt changes occurred along the profile. Although there were small fluctuations due to illumination distribution, surface reflections, and sensor-induced variations, these changes did not create consistent regions below the adaptive threshold profile.

Since the system did not detect repeating low-brightness regions at the same x-axis position, the relevant winding layer was classified as normal. The results indicate that the proposed method provides stable performance under normal winding conditions while maintaining robustness against random brightness fluctuations. The combined evaluation of information from different rows reduced the effect of random brightness variations, resulting in a more reliable system operation.

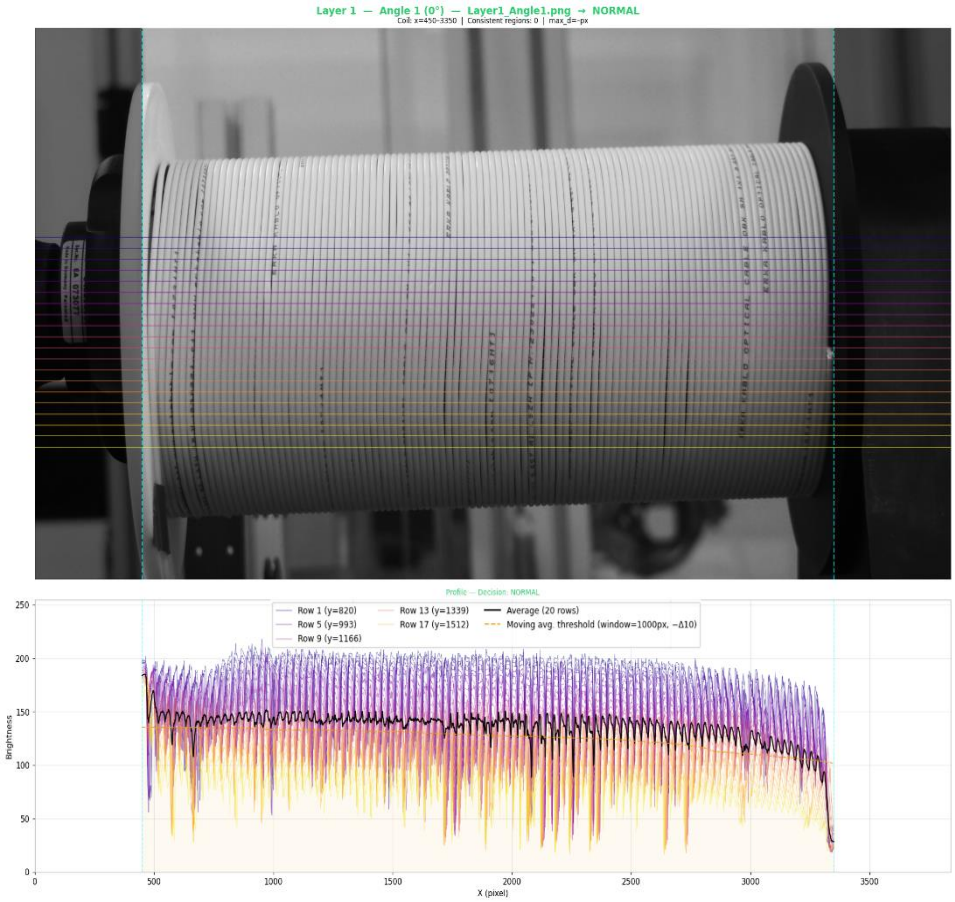

Figure 8. Brightness Profile Analysis Result for a Normal Winding Image (Layer 1, 0°)

4.2. Detection of local winding irregularities

The proposed method was also tested on winding images containing local geometric irregularities. Figure 9 shows the analysis result of the winding image obtained at a 30° angle. The analysis revealed a distinct low-brightness region at approximately x=500 pixels. This region consistently repeated in 12 of the 20 analysis rows, with a maximum region width of 29 pixels. Based on the defined decision thresholds, this was classified as a Fault. Visual inspection revealed an increase in local wire spacing and winding irregularity in the relevant region. The detected low-brightness region corresponds to this physical change.

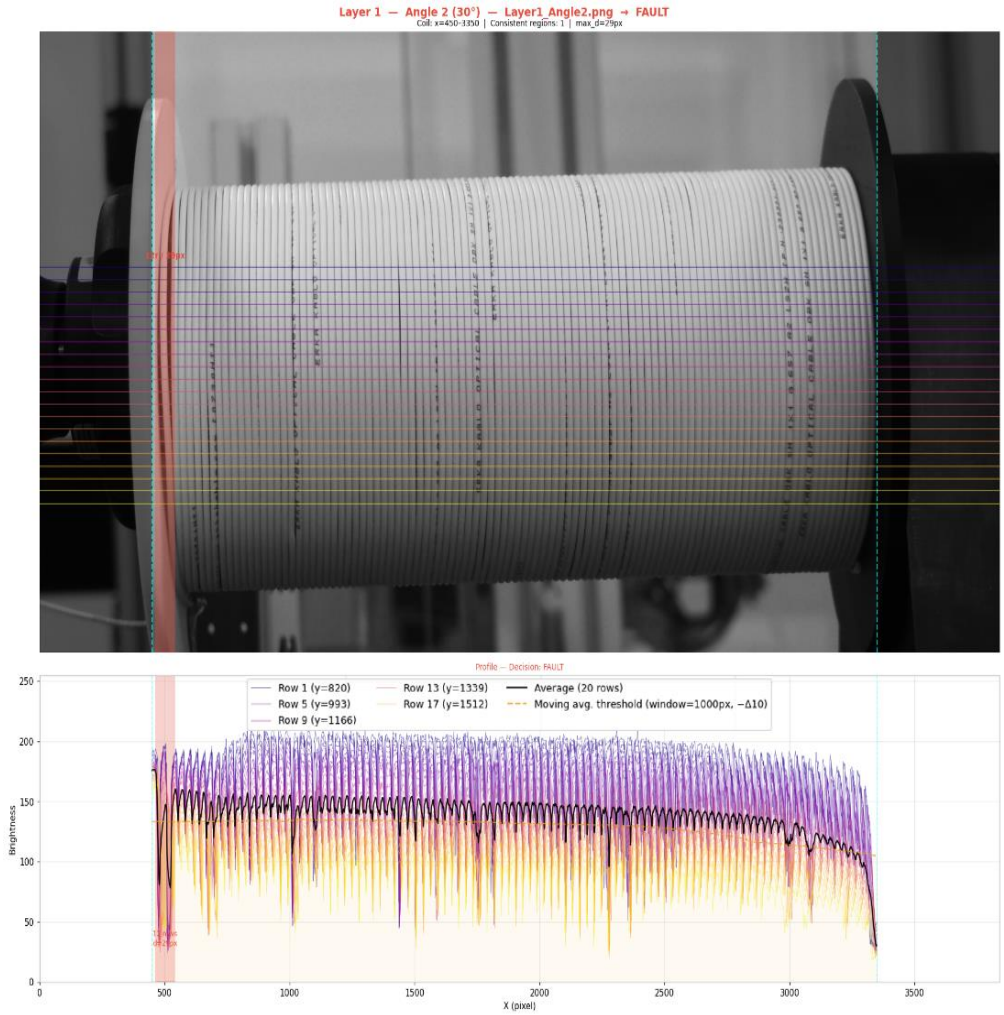

Figure 9. Brightness Profile Analysis Result for a Faulty Winding Image (Layer 1, 30°)

In the image of the same layer obtained at a 300° angle, a different low-brightness region was detected at approximately x = 500 and x = 2700 pixels (Figure 10). The first region was consistently repeated in 14 of the 20 analysis rows, with a maximum region width of 32 pixels. The second region consistently repeated in 11 of the 20 analysis rows, with a maximum region width of 28 pixels. The detection of faults at different x-positions in two different angles demonstrates that the multi-angle imaging approach can comprehensively reveal local irregularities on the coil surface.

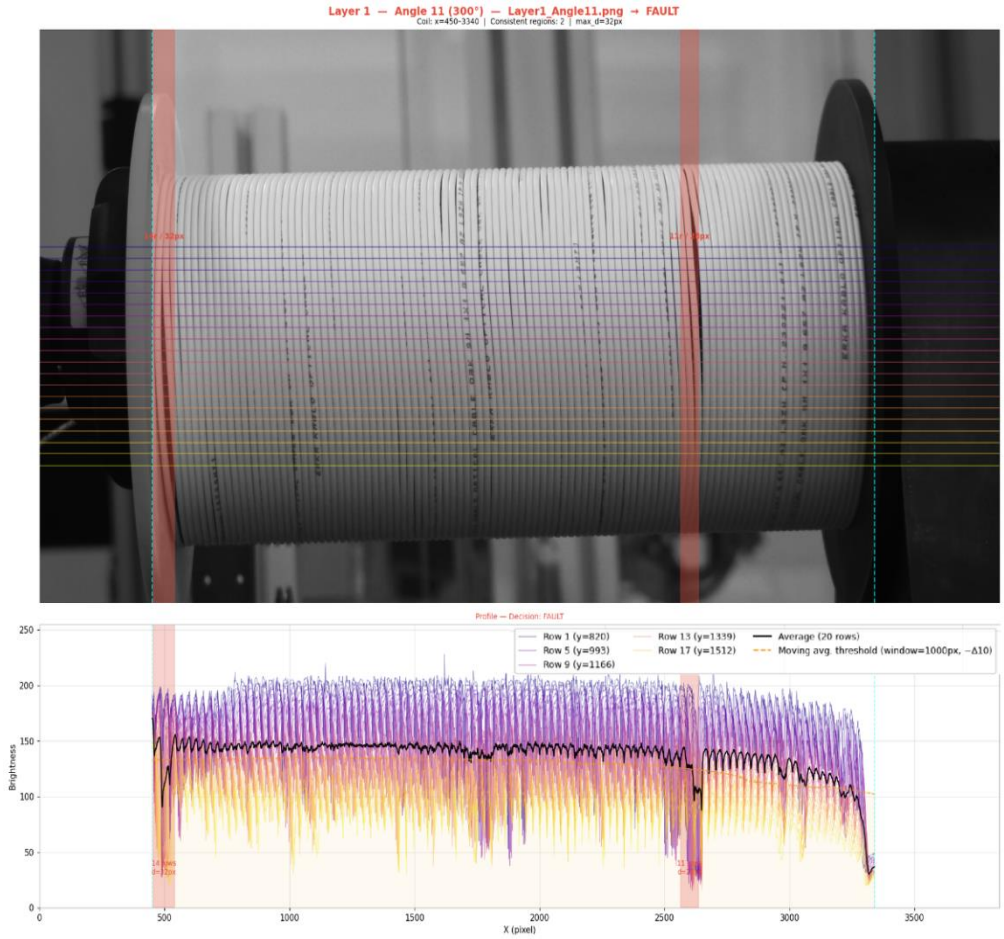

Figure 10. Brightness Profile Analysis Result for a Faulty Winding Image (Layer 1, 300°)

4.3. Layer-level multi-angle analysis results

In the proposed system, layer 1 was analyzed using a total of 12 different angle images obtained at 30° intervals. The analysis results for each angle are given in Figure 11. Examination of the analysis results revealed significant Fault signals at 30°, 270° and 300° angles, and these angles were classified as faults. Local winding irregularities were also observed by the operator at this layer, and the system decision coincides with the physical observation. At 0°, 90°, 150°, 180°, 210°, 240°, and 330° angles, no consistent low-brightness region was detected, and these angles were correctly classified as Normal. At 60° and 120° angles, a Warning decision was given. The consistent region widths detected at these angles exceed the warning threshold but remain below the Fault threshold. It is considered that this situation may be due to several different sources: due to the cylindrical surface geometry and angle-dependent light reflection characteristics, the same physical distortion can manifest itself with different intensities at different angles; in addition, surface glare, local lighting variations, or sensor-generated noise can also cause the threshold value to be partially exceeded. Furthermore, it should not be overlooked that the winding at these angles may be Normal, and the detected signal may be solely due to noise.

The final decision per layer is determined according to the priority rule Fault > Warning > Normal, and the relevant layer is classified as Fault. The operator is only informed when a Fault decision is generated; Normal and Warning decisions are recorded but do not require operator intervention.

The results obtained show that the proposed system can successfully detect local winding irregularities observed by the operator. However, it is not possible to definitively distinguish whether the signals observed at angles where a Warning decision is given originate from a true geometric distortion or from lighting variations and sensor noise. This is considered a current limitation of the system and is planned to be addressed with more comprehensive test data in the future.

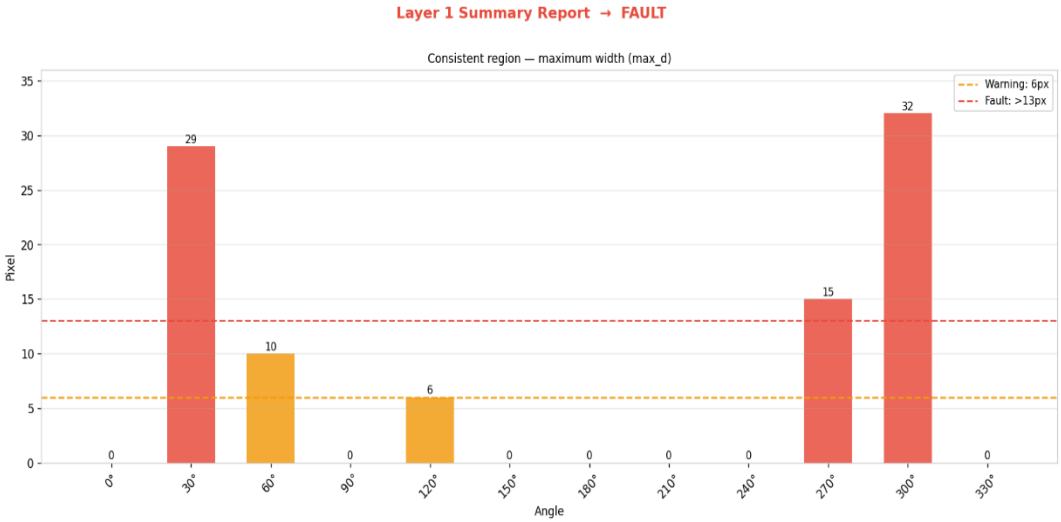

Figure 11. Layer 1 Multi-Angle Analysis Summary

The experimental validation presented in this study was limited to the detection of local winding irregularities characterized by increased spacing between adjacent wires. Although other types of geometric defects, such as wire overlaps and local variations in the winding angle, may also occur during the winding process, these defect categories were not explicitly investigated in the present study. Consequently, the applicability and detection performance of the proposed method with respect to these additional defect types remain to be validated through more comprehensive experimental studies encompassing a broader range of winding irregularities.

To provide a quantitative assessment of the proposed method, a conservative worst-case binary evaluation was additionally performed. Since the proposed method produces three decision categories (Normal, Warning, and Fault), the Warning category represents borderline cases that require further inspection rather than confirmed defects. Accordingly, for the purpose of quantitative performance evaluation, the Warning and Fault categories were combined into a single positive class, whereas the Normal category was considered the negative class.

Table 3. Confusion Matrix for the Binary Performance Evaluation

	System Normal	**Operator Fault**
System Normal	15	0
System Positive (Warning/Fault)	2	3

The quantitative performance evaluation based on the confusion matrix yielded an accuracy of 90.0%, a precision of 60.0%, a recall of 100.0%, a specificity of 88.24%, and an F1-score of 75.0%.

According to the conservative worst-case evaluation, all winding layers classified as Fault by the reference operators were correctly identified by the proposed method, resulting in a recall of 100.0%. Two layers classified as Normal by the operators were assigned to the Warning category by the proposed method and were consequently treated as false positives in the binary evaluation. However, since the Warning category represents borderline cases requiring further inspection rather than confirmed defects, the reported performance metrics should be regarded as a conservative estimate of the actual performance of the proposed method.

As a general assessment of the experimental studies, the proposed quality control system was evaluated using winding images obtained during experimental studies. Images from a total of 20 winding layers were both visually inspected by the operator and analyzed using the proposed algorithm. All significant geometric irregularities detected by the operator were successfully identified by the system. Furthermore, the proposed method demonstrated stable performance in normal winding regions, while Warning decisions were generated only for a limited number of borderline cases. The results demonstrate that the proposed approach can be used as a reliable quality control tool under real production conditions.

Table 4. Layer-Level Quality Assessment: System Decisions and Operator Observations

Layer	System Decision	Operator Assessment
1	Fault	Fault
2	Normal	Normal
3	Warning	Normal
4	Normal	Normal
5	Normal	Normal
6	Normal	Normal
7	Normal	Normal
8	Normal	Normal
9	Normal	Normal
10	Fault	Fault
11	Normal	Normal
12	Normal	Normal
13	Normal	Normal
14	Normal	Normal
15	Normal	Normal
16	Warning	Normal
17	Warning	Fault
18	Normal	Normal
19	Normal	Normal
20	Normal	Normal

As shown in Table 4, a total of 20 winding layers were analyzed; the system correctly identified all layers classified as Fault, and system decisions and operator assessments showed agreement in these layers. No layer assessed as Normal by the operators was directly classified as Fault by the proposed system. However, two Normal layers were classified as Warning and were therefore counted as false positives in the conservative binary evaluation. Warning decisions were given in three layers (Layers 3, 16, and 17). Layer 17 was evaluated as Fault by the operator, indicating that the system detected the relevant irregularity but underestimated its severity. Layers 3 and 16 were evaluated as Normal by the operator; this indicates that the brightness variations remained within the noise tolerance range. Overall, the proposed system demonstrated 85% agreement with operator assessments throughout the 20-layer analysis process.

5. Conclusion and Future Studies

This study proposes an image processing-based quality control system for the online detection of geometric winding defects in sequential fiber optic wire winding devices. The system consists of multi-angle image acquisition, ROI-based multi-row brightness profiling, moving average-based adaptive thresholding, inter-row consistency analysis, and layer-based decision mechanisms. In the experimental studies, images obtained from 12 different angles for each winding layer were analyzed, and it was observed that the system operated stably throughout the 20 layer winding process. The results showed that local geometric irregularities observable by the operator could be successfully detected with the proposed image processing-based method. The quantitative evaluation presented in Table 3 confirms that the system exhibits 85% agreement with operator assessments across all 20 layers analyzed. None of the winding layers classified as Normal by the reference operators was incorrectly classified as Fault by the proposed method. However, two Normal layers were assigned to the Warning category and were consequently treated as false positives in the conservative binary evaluation.

Experimental studies have shown that the proposed method can successfully detect local winding irregularities observed by the operator. Thanks to multi-row consistency analysis, singular brightness drops caused by sensor noise and local illumination variations are eliminated, and true geometric distortions are reliably detected. The multi-angle imaging strategy prevents the overlooking of local winding defects that become visible only at certain angles. Unlike traditional methods, the system operates online when each winding layer is completed and only informs the operator when a fault decision is generated. The experimental results presented in this study were obtained using a 2 mm diameter fiber optic wire.

The main limitations of the current method can be summarized as follows: due to its intensity-based operation, subtle geometric distortions that do not significantly change the average brightness level are sometimes not detected. Furthermore, it is not possible to definitively distinguish whether the signals observed at the warning angles are due to a true geometric distortion or to variations in lighting and sensor noise. The proposed method was experimentally validated using a single fiber optic coil comprising 20 winding layers. Although a total of 240 images, corresponding to 12 angular views per layer, were analyzed, the final quality assessment was performed at the layer level. Consequently, the performance evaluation was based on 20 independent layer-level observations rather than 240 image-level observations. Accordingly, the results presented in this study should be considered as an initial experimental validation of the proposed method. Further validation through more comprehensive experiments involving multiple coils, a larger number of winding layers, diverse operating conditions, and a wider variety of defect types is necessary to establish the generalizability and robustness of the proposed method. Overall, the proposed system offers a practical, low-cost, and non-destructive solution for

online monitoring of winding quality. By combining a multi-angle imaging approach with brightness profile analysis and adaptive thresholding, it has been shown that local winding defects can be reliably detected without the need for large training datasets or complex computational methods.

Future studies could address the following topics:

- Fully automating the ROI determination process.
- Comprehensive testing of the system with images of more layers and different defect types and calculation of validation metrics.
- Comparing deep learning-based approaches with the current method.
- Improving fine defect detection with higher resolution imaging.
- Testing the generalizability of the system in coils with more different wire diameters and winding parameters.
- Optimizing processing time for real-time integration.

Acknowledgments

The authors thank those who contributed to this study. During the preparation of this article, the authors used Claude (Anthropic, Sonnet 4.6) only for language formatting and the creation of specific explanatory figures (Figure 1 and Figure 4) based on the authors' original data and design. All scholarly content, analysis, and conclusions are the authors' original work, and the authors are fully responsible for the accuracy and integrity of the article.

Author Contributions

Conceptualization: T.A.; methodology: T.A.; software: T.A.; validation: T.A., E.E.; formal analysis: T.A.; investigation: T.A.; data curation: T.A.; writing—original draft preparation: T.A.; writing—review and editing: S.O., E.E.; visualization: T.A.; supervision: S.O. All authors have read and agreed to the published version of the manuscript.

Data Availability Statement

The data that support the findings of this study are available from the corresponding author upon reasonable request.

Conflict of Interest

The authors declare no conflict of interest.

Ethical Approval

This article does not contain any studies with human participants or animals performed by the authors.

References

Chen, X., Liu, N., You, B., & Xiao, B. (2016). A novel method for surface defect inspection of optic cable with short-wave infrared illuminance. Infrared Physics & Technology, 77, 456–463. https://doi.org/10.1016/j.infrared.2016.07.001

Gou, S., Huang, D., Liao, S., Luo, F., Yuan, Y., Liu, L., & Wen, X. (2024). Online defect detection method of optical cable pitch based on machine vision technology and deep learning algorithms. Optics & Laser Technology, 171, 110344. https://doi.org/10.1016/j.optlastec.2023.110344

Grün, V. A., Dyagilev, A., Greb, C., & Gries, T. (2025). Inline quality control of filament wound composite overwrapped pressure vessels. Journal of Composites Science, 9(12), 690. https://doi.org/10.3390/jcs9120690

Guo, C., & Yang, R. (2014). The improved defects detection method of optical fiber winding. Optik, 125(2), 675–678. https://doi.org/10.1016/j.ijleo.2013.07.054

Hung, J. Y., & White, H. V. (1992a). Precision winding of fiber optic filament. I. Winding characteristics. IEEE Transactions on Industrial Electronics, 39(3), 258–267. https://doi.org/10.1109/41.141628

Hung, J. Y., & White, H. V. (1992b). Precision winding of fiber optic filament. II. Winding control. IEEE Transactions on Industrial Electronics, 39(4), 313–321. https://doi.org/10.1109/41.149749

Moru, D. K., & Borro, D. (2020). A machine vision algorithm for quality control inspection of gears. The International Journal of Advanced Manufacturing Technology, 106(1–2), 105–123. https://doi.org/10.1007/s00170-019-04426-2

Rasheed, A., Zafar, B., Rasheed, A., Ali, N., Sajid, M., Dar, S. H., Habib, U., Shehryar, T., & Mahmood, M. T. (2020). Fabric defect detection using computer vision techniques: A comprehensive review. Mathematical Problems in Engineering, 2020, Article 8189403. https://doi.org/10.1155/2020/8189403

Siddiqui, S. Z. N., Qadir, M. U., ul Haq, I., Shah, K., Afridi, M. T., & ur Rehman, S. (2020). Design of precision fiber optic winding machine based on fuzzy logic control system. In 2020 International Conference on Electrical, Communication, and Computer Engineering (ICECCE) (pp. 1–5). IEEE. https://doi.org/10.1109/ICECCE49384.2020.9179332

Tang, B., Chen, L., Sun, W., & Lin, Z.-K. (2023). Review of surface defect detection of steel products based on machine vision. IET Image Processing, 17(2), 303–322. https://doi.org/10.1049/ipr2.12647

Xu, J., Zheng, S., Sun, K., & Song, P. (2023). Research and application of contactless measurement of transformer winding tilt angle based on machine vision. Sensors, 23(10), 4755. https://doi.org/10.3390/s23104755

Zhang, G., Tang, Z., Fan, Y., Liu, J., Jahanshahi, H., & Aly, A. A. (2021). Steel wire rope surface defect detection based on segmentation template and spatiotemporal gray sample set. Sensors, 21(16), 5401. https://doi.org/10.3390/s21165401

Zhang, X., Yang, J., Qian, Y., Zhang, Z., Wang, X., & Xue, Y. (2024). An identification of collapse defect in fiber optic winding structure based on distributed stress testing. Journal of Lightwave Technology, 42(5), 1667–1674. https://doi.org/10.1109/JLT.2023.3324842

Zhao, X., Wang, Y., Kang, Y., Hu, S., Guan, C., Guo, W., Lian, Z., & Liang, S. (2024). Defect recognition in fiber-optic coil winding based on improved MobileNetV1. IEEE Sensors Journal, 24(17), 27300–27308. https://doi.org/10.1109/JSEN.2024.3430030

Zhou, Y., Yuan, M., Zhang, J., Ding, G., & Qin, S. (2023). Review of vision-based defect detection research and its perspectives for printed circuit board. Journal of Manufacturing Systems, 70, 557–578. https://doi.org/10.1016/j.jmsy.2023.08.019

Zhuo, Q., Kong, L., Zheng, J., Ding, Z., Li, W., Yi, D., & Lian, G. (2024). Real-time batch detection system for defects in highly curved spiral cylindrical coils. IEEE Access, 12, 153370–153384. https://doi.org/10.1109/ACCESS.2024.3448630